Supporting Information

Theoretical study on reduction mechanism of CO_2 to HCOOH on Pd_3Au: An explicit solvent model is essential

Ming Zheng[1], Xin Zhou[1*], Yixin Wang[1], Gang Chen[1], Mingxia Li[2*]

[1]MIIT Key Laboratory of Critical Materials Technology for New Energy Conversion and Storage, School of Chemistry and Chemical Engineering, Harbin Institute of Technology, Harbin150001 P. R. China

[2]School of Chemistry and Materials Science, Key Laboratory of Functional Inorganic Material Chemistry, Ministry of Education of the People's Republic of China, Heilongjiang University, Harbin 150080, PR China

*Corresponding author: zhoux@hit.edu.cn and limingxia@hlju.edu.cn

Computational methods and model

Free energy corrections

In searching for possible thermodynamic routes, all free energies (ΔG) were calculated by the following equation:

$\Delta G = \Delta E_{DFT} + \Delta ZPE - T\Delta S$

where ΔE_{DFT} is the energy difference between reactants and products, obtained from DFT calculations; ΔZPE and ΔS are the energy differences in zero-point energy and entropy; T is 298.15 K. ZPE of all adsorbates were calculated from Vibrational analysis, limited to the surface species and keeping the rest of the system fixed, was carried out by calculating the Hessian matrix with a finite difference approach with a step size of 0.015 Å. Vibrational contributions to the entropies for substrate were

considered to be inconsequential and counted as zero in the part of TΔS. For molecules, the vibrational contributions to the entropies were calculated from standard thermodynamic tables at 298.15 K and 1 atm. The proton electron pairs transfer energy involved in the reaction pathway is solved by using the computational hydrogen electrode model.

Adsorption energy

Various intermediates adsorbed on different sites on the surface were considered. Generally, the adsorption sites can be classified into three types: top, bridge, and hollow sites. Hollow site includes fcc-like and hcp-like sites in close-packed crystal structure.

Adsorption energy is calculated by the following equation:

$$\Delta E_{ads} = E_{adsorbate\text{-}slab} - E_{adsorbate} - E_{slab}$$

$E_{adsorbate\text{-}slab}$ is the total energy of molecules or intermediates adsorbed on the slab surface, $E_{adsorbate}$ and E_{slab} are energies for the isolated adsorbate and slab, respectively. It was worth noting that the intermediates are rarely adsorbed on the Au-related site, indicating that catalytic active sites were near the Pd atom. Meanwhile, the adsorption energies of fcc-like or hcp-like site were close, suggesting that the second layer has no obvious effect on the adsorbates.

Slab model

In theoretical research, the Au-Pd system compounds were found at the experimentally known compositions. The UPb[1, 2] prototype structure (Nr40[3]) is predicted the most stable phase for AuPd. But experimental proof for the existence of this structure is still lacking, probably due to the low order-disorder temperature. The phase diagram of the Au-Pd system has ordered $L1_2$ structures ($L1_2$ is index by Strukturbericht designation and the prototype is $AuCu_3$ structure) for Au_3Pd and $AuPd_3$ compositions, which already identified by experiment.[4]

In the experiment, Marco Valenti et al[5] measured the faradaic efficiencies for H_2

of the five synthesized Pd-Au alloy electrodes at −0.5 V vs RHE. The faradaic efficiencies for H_2 in $Au_{25}Pd_{75}$ is the minimum, which indicating $Au_{25}Pd_{75}$ could effective suppresses H_2 evolution reaction (HER). In addition, with the increasing the Pd content, the partial current density of H_2 decreases, which also indicate $Au_{25}Pd_{75}$ could effectively suppress HER. It can thus be seen, when the Pd Au ratio was 1:3, the material could effectively suppress HER.

The surface segregation of Pd-Au system is a complex process, which is affected by many factors (such as temperature=e and adsorption molecule[6, 7]). Dragana D et al.[8] found that in the case of CO adsorption, the Au surface segregation of Pd_3Au (111) becomes endothermic, which indicates that the surface maintains a bulk composition in the presence of CO. In addition, it is reported that the surface enrichment of PdAu nano-clusters in the presence of CO is observed by Diffuse Reflectance Infrared Fourier Transform Spectroscopy (DRIFTS), and DFT calculations show that Pd atoms prefer to low-coordination at the edges of nano-clusters[6]. Gao et al. reported similar results using polarization modulated infrared reflectance absorption spectroscopy (PM-IRAS). When the CO pressure is higher than ~0.1 Torr, Pd segregation is greatly enhanced, forming continuous Pd sites[7]. However, some experimental reports have shown that surface atoms do not segregate in the presence of strongly adsorbed species during the CO_2RR. Marco Valenti et al[5] collected XPS spectra of PdAu alloys before and after electrolysis at −0.5 V vs RHE for 20 min. The results show that there are no significant changes in the shape of the valence band are noted, which suggests that no phase segregation occurred during the reaction that could affect the local electronic properties of the electrode surface. In addition, the CV spectrum shows that the reduction peaks of the alloy do not overlap with the pure components, indicating that there is no region containing pure Au or Pd on the surface of the alloy electrode. It can be seen that the segregation of alloys is very complex, especially in the electrochemical environment. In this wok, we mainly explore the mechanism of CO_2 reduction on specific electronic structure PdAu alloys, even though partial segregation of surface atoms in really experiment possible, the material still retains its specific electronic structure. Thus, the Pd-Au slab model without segregation was used in this work.

Potential-dependent kinetic barrier

According to Chan and Nørskov[9, 10], as long as there is excess charge on the electrode, the potentials applied would show some effect on the activation energies. Thus, we adopt this method to compute the barriers for on the Pd_3Au (111) surface at different potentials. The parameters for determining the potential-dependent kinetic barriers for non-electrochemical reaction steps in this work were shown in Table S3. In this method, the key assumption is that the electrical double layer at the electrode surface can be approximated by a capacitor model. The relationship of a constant-charge reaction free energy to a constant-potential reaction free energy is shown below:

$$G_2(\Phi_1) - G_1(\Phi_1) = G_2(\Phi_2) - G_1(\Phi_1) + (q_2 - q_1) \times (\Phi_2 - \Phi_1)/2 \quad (1)$$

$$G_2(\Phi_2) - G_1(\Phi_2) = G_2(\Phi_2) - G_1(\Phi_1) - (q_2 - q_1) \times (\Phi_2 - \Phi_1)/2 \quad (2)$$

in which $G_1(\Phi_1)$ and $G2(\Phi2)$ represent the free energies or active barriers, which directly from the DFT calculation. "1" and "2" denote two different states, for example, "1" could be an IS, "2" could be a TS or FS, and q_1 and q_2 are the excess surface charges, at states 1 and 2 simulated with constant charge (where calculated by a Bader charge analysis[11, 12]), the Φ is the work function. We computed the work function (Φ) of each state by taking the difference between the vacuum level and the system's Fermi level.

The two data points derived via Eq. (1) and Eq. (2) allow us to establish the linear dependence of G on Φ (as shown in Figure S10 and S11), so that we can compute the reaction free energy at any work function.

Solvation model

When calculating thermodynamic paths, to observe interaction of various intermediates with water, continuum solvation modeling in VASPsol code[13, 14] was employed in this work. This implicit solvation includes the effect of electrostatics, cavitation, and dispersion on the interaction of metal surface and water.

AIMD simulation

To evaluate the effect of dynamic h-bond network on activation energy barrier, the ab initio molecular dynamics (AIMD) with a "slow-growth" method[15-17] was used to sample the free energy profile. In AIMD simulation, the 40 H_2O molecules were putted on Pd_3Au (111) surface, the supercell dimensions are 19.283 Å, 11.133 Å and 21.356 Å. For Pd_3Au (211) surface, we put 30 H_2O molecules in 13.239 Å, 10.852 Å, and 21.383 Å supercells to simulate three layers of water molecules. All constrained molecular dynamics were performed Vienna Ab initio Simulation Package (VASP)[18, 19]. The cutoff energy of the plane-wave basis is 400 eV in the AIMD simulations. The 2×2×1 Gamma-centered k-mesh is used in Pd_3Au (211) surface and 1×2×1 Gamma-centered k-mesh is used in Pd_3Au (111) surface. Time step in MD is set to be 0.5 femtosecond. Projector-augmented wave (PAW) was used to account for core-valence interactions,[20, 21] within the exchange-correlation function was described by Perdew, Burke, and Ernzerhof (PBE)[22]. The D3 correction of Grimme[23, 24] was adopted to compensate for the lack of van der Waals interaction description in the GGA functional. The dynamic h-bond network model of Pd_3Au (111) surface were shown in Figure S16.

Table S1. The atom's net charge calculated by the Bader charge analysis. (Net charge = Valence charge − Total Bader charge, the valence charges of Pd and Au are 10 and 11, respectively.)

	Top layer				2nd layer			
	100	110	111	211	100	110	111	211
Pd	-0.016	0.027	-0.023	-0.053	-0.093	-0.058	-0.069	-0.080
Au	0.164	0.085	0.160	0.156	—	—	0.175	0.123
Total	1.330	1.010	0.361	0.390	-1.679	-1.050	-0.395	-0.467

Table S2 The most favorable adsorption site, main bond length, adsorption distance ($d_{slab\text{-}adsorbate}$), adsorption energies ($E_{ads}$) and atom's net charge for the Pd_3Au (111), (1 0 0), (1 1 0) and (2 1 1) surfaces. The units for bond length and adsorption energy are Å and eV, respectively.

	Pd_3Au (111)		Pd_3Au (100)		Pd_3Au (110)		Pd_3Au (211)	
CO_2*	site	t	site	t	site	t	site	t
	$d_{slab\text{-}adsorbate}$	3.145	$d_{slab\text{-}adsorbate}$	3.137	$d_{slab\text{-}adsorbate}$	3.233	$d_{slab\text{-}adsorbate}$	3.218
	C-O	1.177	C-O	1.177	C-O	1.178	C-O	1.177
	C-O	1.177	C-O	1.177	C-O	1.177	C-O	1.178
	$E_{ads.}$	-0.308	$E_{ads.}$	-0.315	$E_{ads.}$	-0.213	$E_{ads.}$	-0.365
	net charge	0.037	net charge	0.039	net charge	0.036	net charge	0.151
COOH*	site	h	site	t	site	b	site	t
	$d_{Pd\text{-}C}$	2.151	$d_{Pd\text{-}C}$	1.989	$d_{Pd\text{-}C}$	1.969	$d_{Pd\text{-}C}$	1.989
	$d_{Pd\text{-}O}$	2.224			$d_{Pd\text{-}O}$	2.187		
	C-O	1.353	C-O	1.342	C-O	1.351	C-O	1.353
	C-O	1.257	C-O	1.212	C-O	1.238	C-O	1.195
	$E_{ads.}$	-2.397	$E_{ads.}$	-2.377	$E_{ads.}$	-2.746	$E_{ads.}$	-2.536
	net charge	0.196	net charge	0.028	net charge	0.134	net charge	0.043
HCOO*	site	t	site	t	site	t	site	t
	$d_{Pd\text{-}C\ C}$	2.145	$d_{Pd\text{-}C}$	2.153	$d_{Pd\text{-}C}$	2.084	$d_{Pd\text{-}C}$	2.150
	$d_{Pd\text{-}C}$	2.146	$d_{Pd\text{-}C}$	2.174	$d_{Pd\text{-}C}$	2.083	$d_{Pd\text{-}C}$	2.165
	C-O	1.269	C-O	1.268	C-O	1.267	C-O	1.271
	C-O	1.269	C-O	1.269	C-O	1.267	C-O	1.271
	$E_{ads.}$	-2.592	$E_{ads.}$	-2.473	$E_{ads.}$	-2.854	$E_{ads.}$	-2.523
	net charge	0.490	net charge	0.496	net charge	0.483	net charge	0.487
HCOOH*	site	t	site	t	site	t	site	t
	C-O	1.349	C-O	1.354	C-O	1.345	C-O	1.351
	C-O	1.216	C-O	1.210	C-O	1.219	C-O	1.220
	$d_{slab\text{-}adsorbate}$	2.456	$d_{slab\text{-}adsorbate}$	2.125	$d_{slab\text{-}adsorbate}$	2.259	$d_{slab\text{-}adsorbate}$	2.454
	$E_{ads.}$	-0.534	$E_{ads.}$	-0.502	$E_{ads.}$	-0.581	$E_{ads.}$	-0.674
	net charge	-0.040	net charge	0.039	net charge	-0.057	net charge	0.039
CO*	site	h	site	b	site	b	site	h

	d_{Pd-C}	2.065	d_{Pd-C}	1.953	d_{Pd-C}	2.028	d_{Pd-C}	2.063
	d_{Pd-C}	2.066	d_{Au-C}	2.126	d_{Pd-C}	2.025	d_{Pd-C}	2.065
	d_{Pd-C}	2.072	$d_{slab-adsorbate}$				d_{Pd-C}	2.051
	C-O	1.192	C-O	1.175	C-O	1.187	C-O	1.206
	$E_{ads.}$	-2.225	$E_{ads.}$	-1.656	$E_{ads.}$	-1.913	$E_{ads.}$	-2.204
	net charge	0.209	net charge	0.102	net charge	0.166	net charge	0.216

Table S3 Parameters for determining the potential-dependent kinetic barriers (eV) for all non-electrochemical steps in this work.

Index	surface	Reaction Steps	Δq(TS-IS)	Δq(FS-IS)	ΔΦ(TS-IS)	ΔΦ(FS-IS)	E_{act} (0 V)	E_{act} (-0.4/-0.33 V)
1	111	CO_2 →COOH	-0.28	-0.39	0.00	-0.01	0.71	0.30
2		CO_2 →HCOO	-0.10	-0.08	-0.02	-0.04	0.96	0.92
3		COOH →HCOOH	-0.12	-0.12	0.05	-0.08	0.58	0.53
4		HCOO →HCOOH	-0.20	-0.60	0.03	-0.06	0.64	0.56
5	211	CO_2 →COOH	-0.31	-0.33	-0.04	0.01	0.55	0.46
6		CO_2 →HCOO	-0.04	-0.02	-0.01	-0.11	0.51	0.49
7		COOH →HCOOH	0.20	0.17	0.11	-0.18	0.53	0.45
8		HCOO →HCOOH	-0.27	-0.58	-0.03	-0.10	0.54	0.44

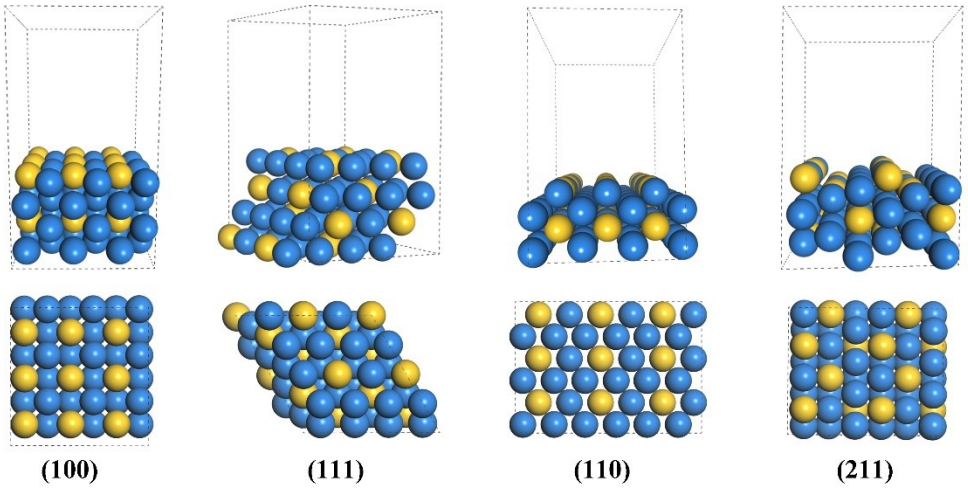

Figure S1 The optimized structures of different Pd_3Au facets (the blue ball represents Pd atom and yellow ball represents Au atom).

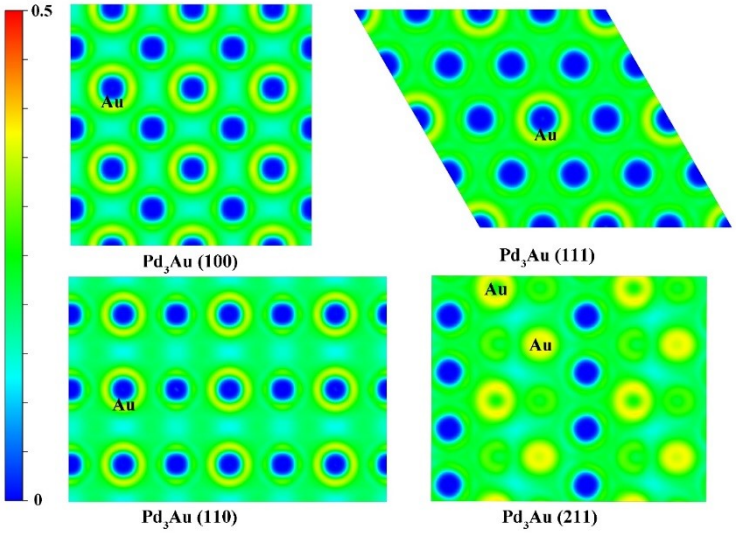

Figure S2 The isosurface of electron localization function on the Pd_3Au (100), (111), (110) and (211) surface. (isosurface level = 0.5)

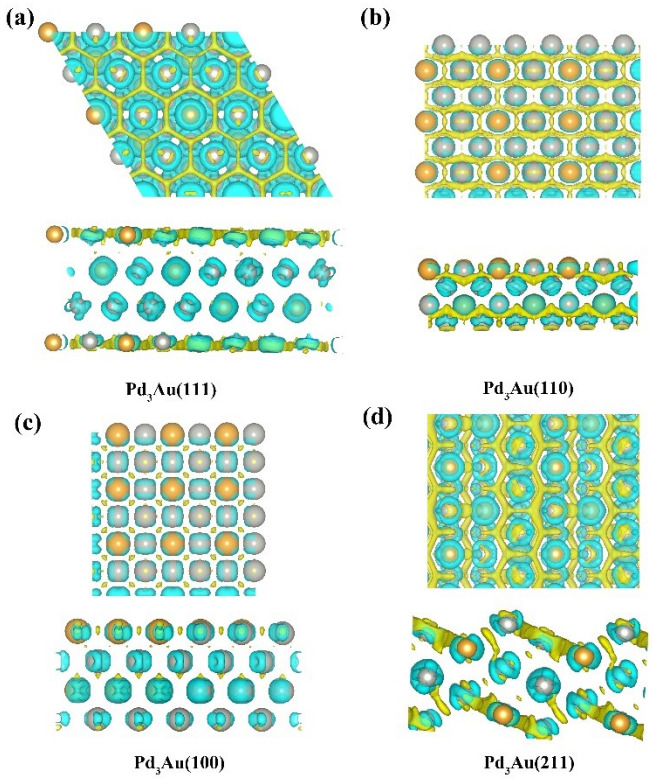

Figure S3 The deformation charge density distribution of the Pd_3Au (100), (111), (110) and (211) surface. Yellow and blue areas denote electron accumulation and depletion, respectively, with isosurface values of 5×10^{-5} e/Å^3

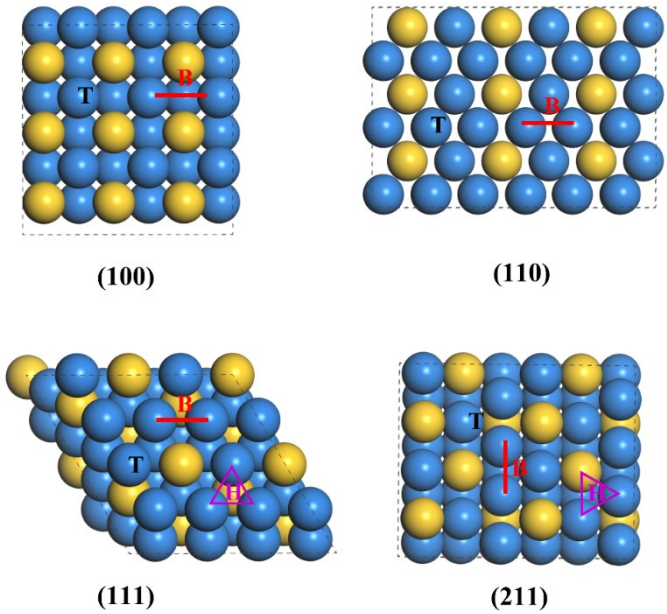

Figure S4 The top views of (1 1 1), (1 0 0), (1 1 0) and (2 1 1) facet surface structure of Pd_3Au. The investigated adsorption sites are marked by different letters in the top views. (The blue ball represents Pd atom and yellow ball represents Au atom, and the adsorption sites can be classified into three types: top (" T "), bridge (" B "), and hollow (" H ") sites)

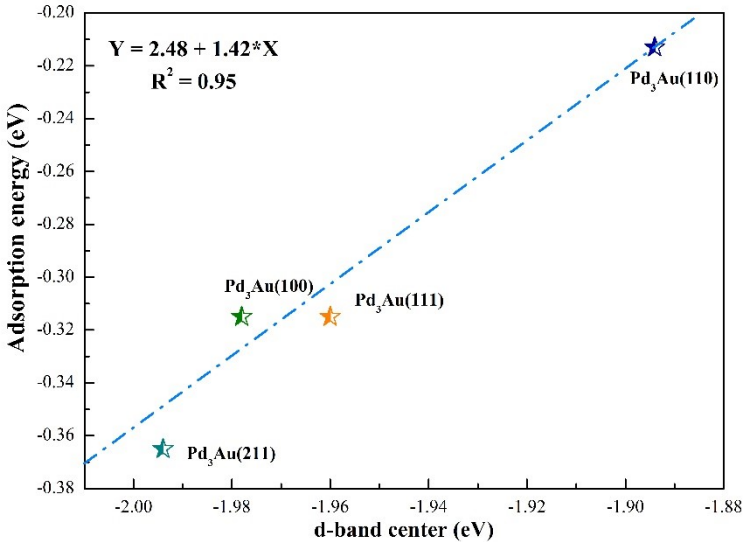

Figure S5 The relationship for Pd_3Au surfaces between d-band center and adsorption energy of CO_2.

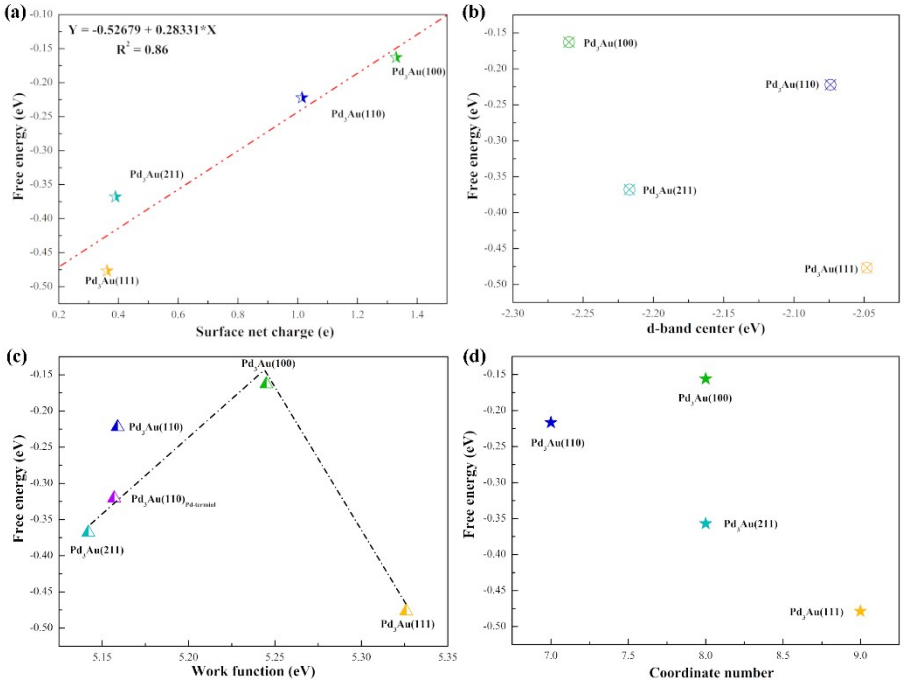

Figure S6 The relationship for Pd_3Au surfaces between ΔG_{H*} and (a) the surface net charge, (b) d-band center (c) the work function, (d) the coordination number.

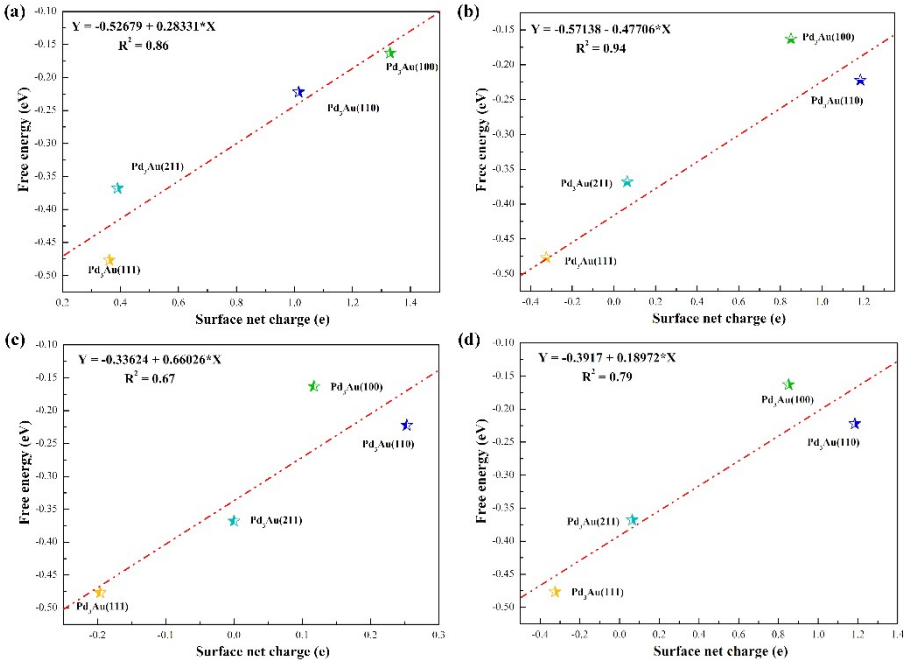

Figure S7 The relationship between the surface net charge (a) Bader charge, (b) DDEC6 charge (c) Hirshfeld charge, (d) Hirshfeld-I charge and Gibbs free energy.

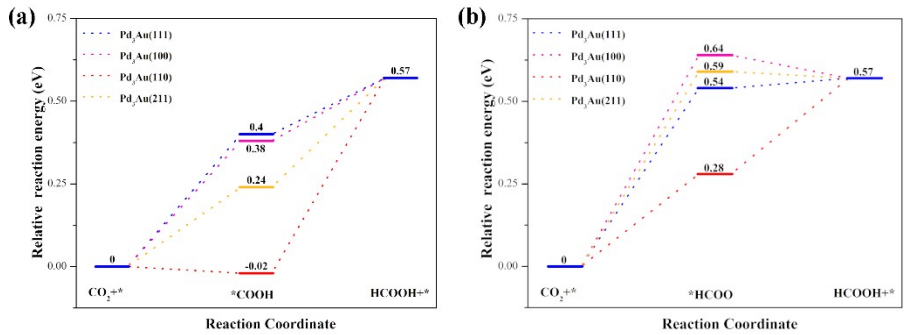

Figure S8 The energy diagram of reduction CO_2 to HCOOH via (a)COOH* and (b) HCOO* routes at the zero-electrode potential (U = 0 V);

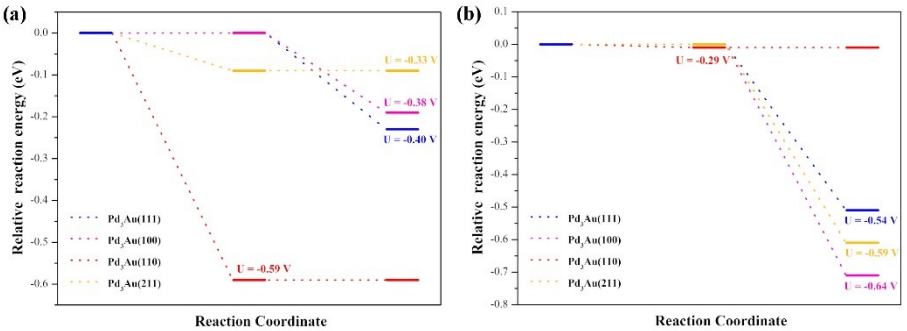

Figure S9 The (a) COOH* and (b) HCOO* routes at the onset potential over Pd_3Au (1 1 1), (1 0 0), (1 1 0) and (2 1 1) surfaces, respectively.

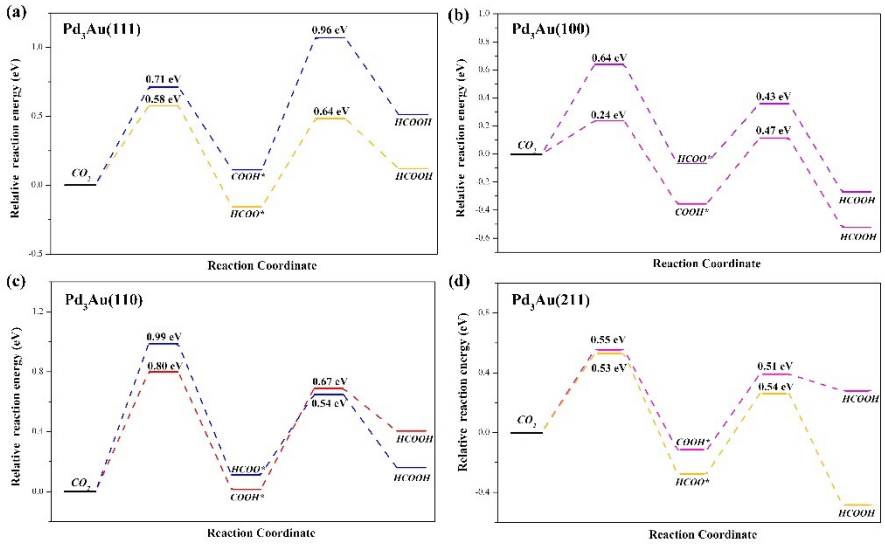

Figure S10 Kinetic barrier diagram for formic acid production on (a) Pd_3Au (111), (b) Pd_3Au (100), (c) Pd_3Au (110), (d) Pd_3Au (211).

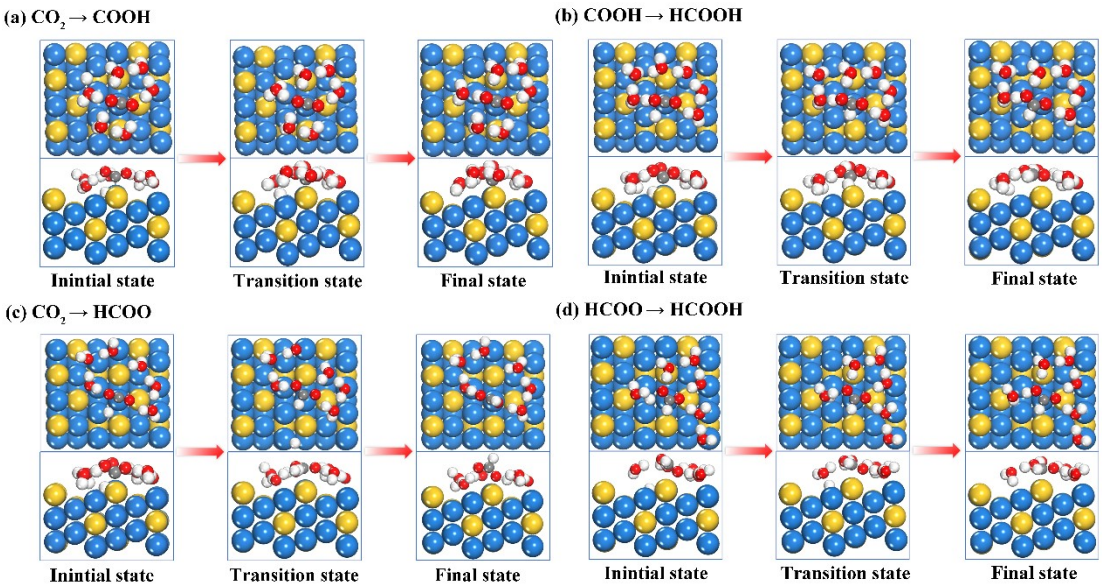

Figure S11 Optimized structures of the initial, transition, and final states involved in (a) COOH* route and (b) HCOO*route on Pd_3Au (211).

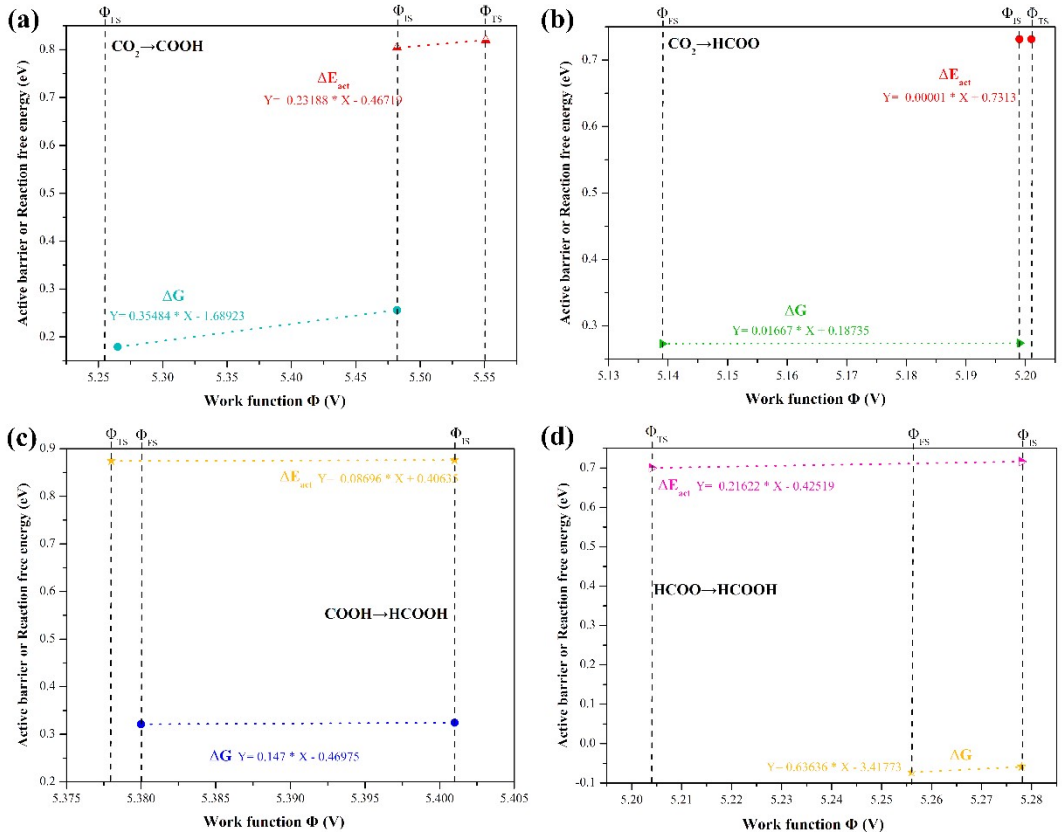

Figure S12. Potential-dependent reaction free energy (ΔG) and activation barrier (ΔE_{act}) on Pd_3Au (111) for (a) CO_2 →COOH, (b) CO_2 →HCOO, (c) COOH → HCOOH, (d) HCOO → HCOOH.

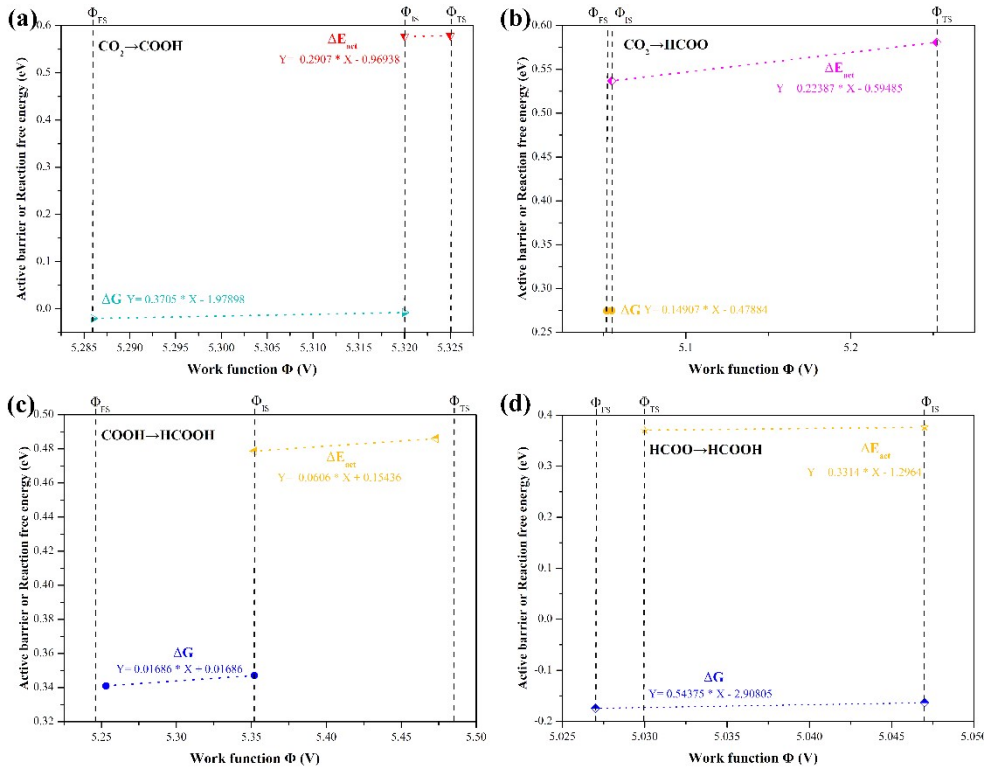

Figure S13. Potential-dependent reaction free energy (ΔG) and activation barrier (ΔE_{act}) on Pd_3Au (211) for (a) CO_2 →COOH, (b) CO_2 →HCOO, (c) COOH → HCOOH, (d) HCOO → HCOOH.

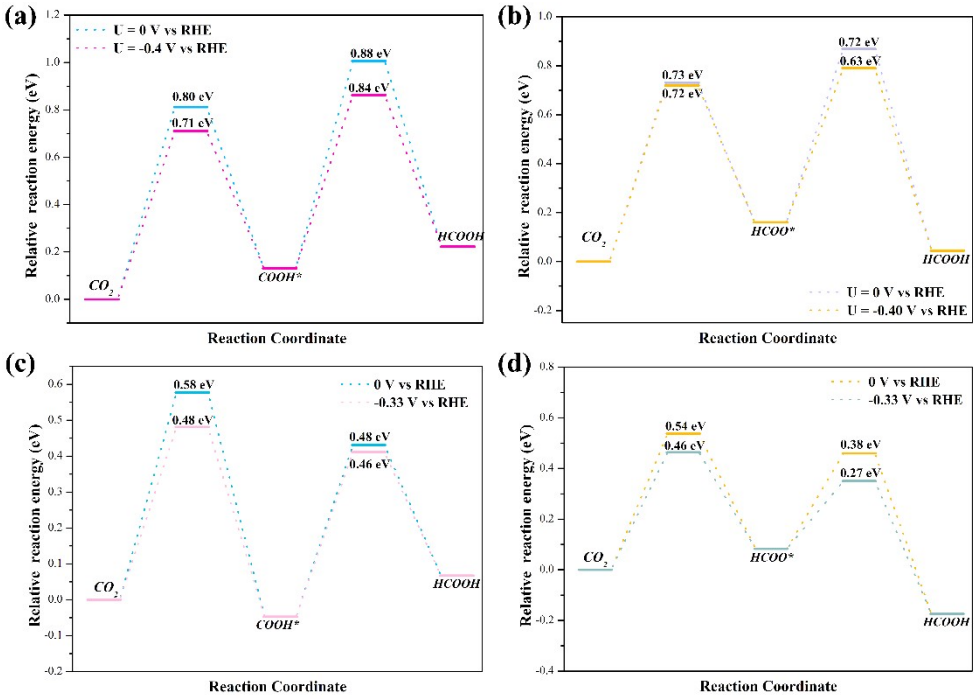

Figure S14 The path of HCOOH formation on the Pd_3Au (111) surface through (a) COOH* routes and (b) HCOO* routes at 0 V and -0.40 V vs RHE; The path of HCOOH formation on the Pd_3Au (211) surface through (c) COOH* routes and (d) HCOO* routes at 0V and -0.33 V vs RHE.

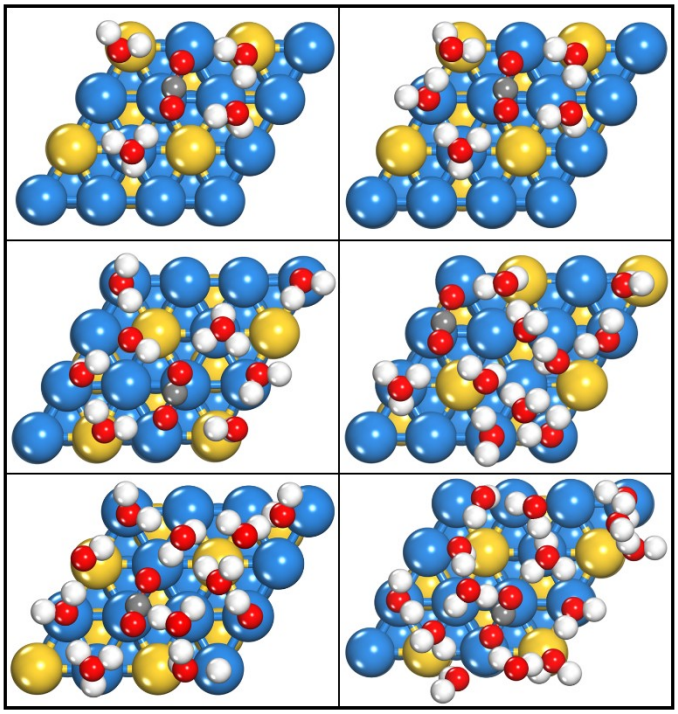

Figure S15 The Transition state structure of $CO_2 + H^+ + e^- \rightarrow$ COOH* with different water molecules model on Pd_3Au (111).

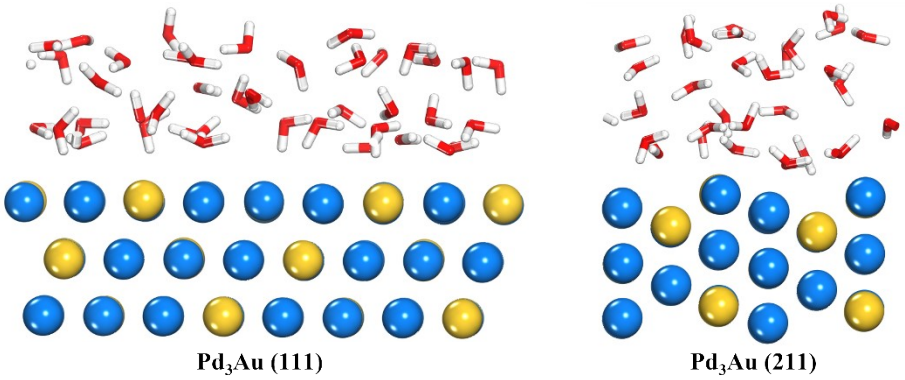

Figure S16 The dynamic h-bond network model of Pd_3Au (111) and (211) surface

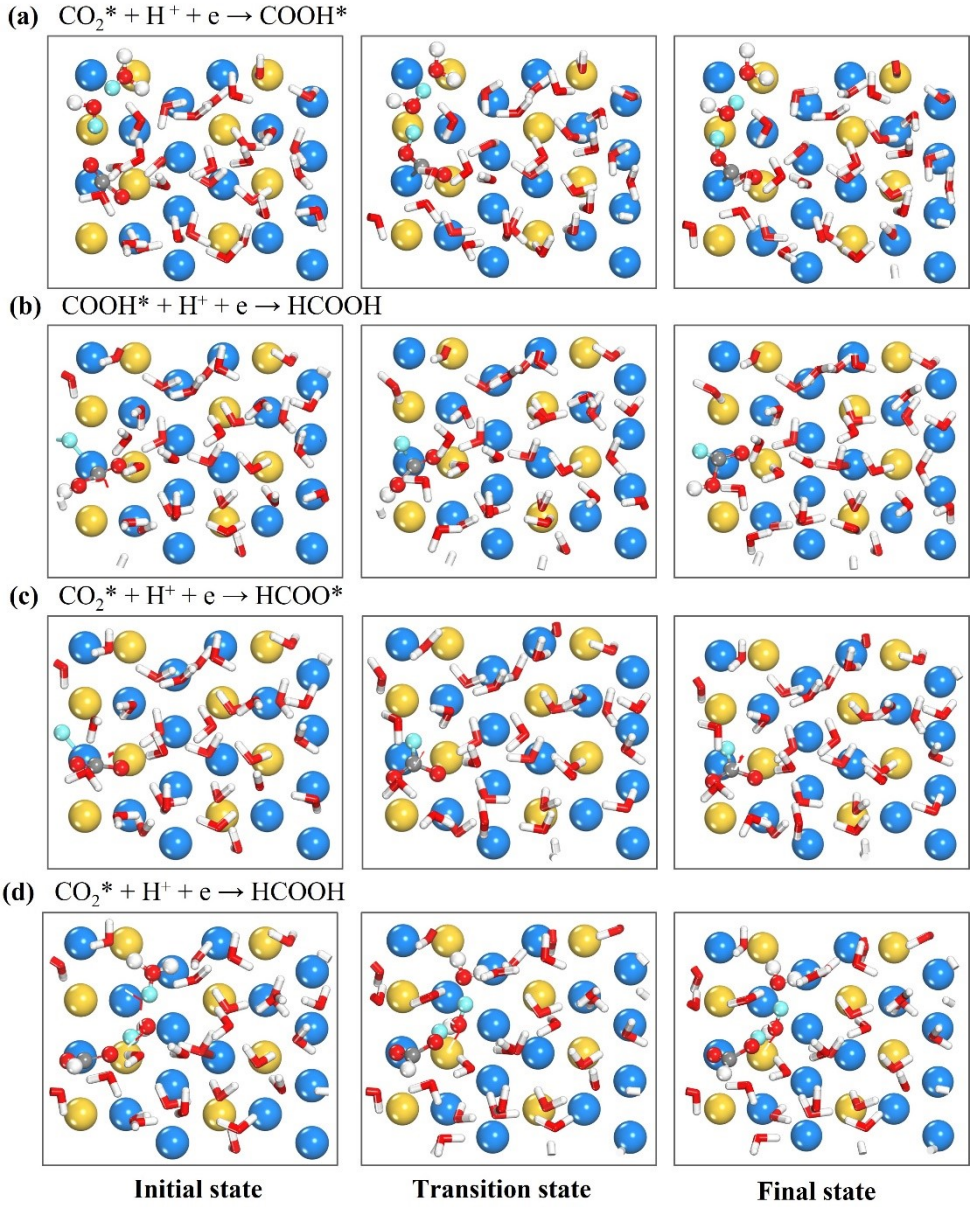

Figure S17 Representative snapshots of the structural evolution of (a) CO_2* → COOH*, (b) COOH* → HCOOH, (c) CO_2* → HCOO*, and (d) HCOO* → HCOOH on Pd_3Au (211).

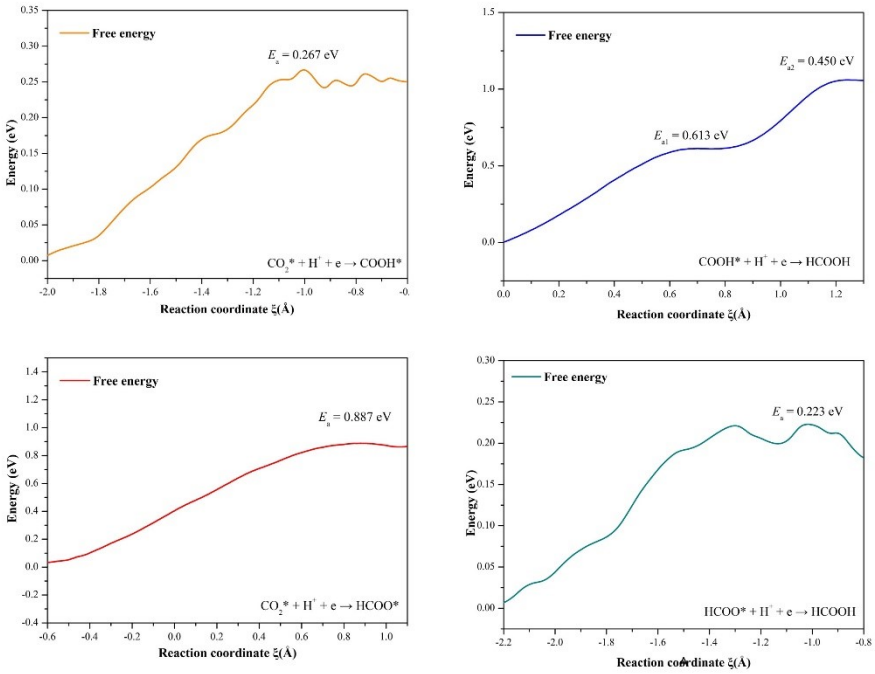

Figure S18 The free energy profiles obtained by integration along the reaction coordinate on Pd_3Au (111).

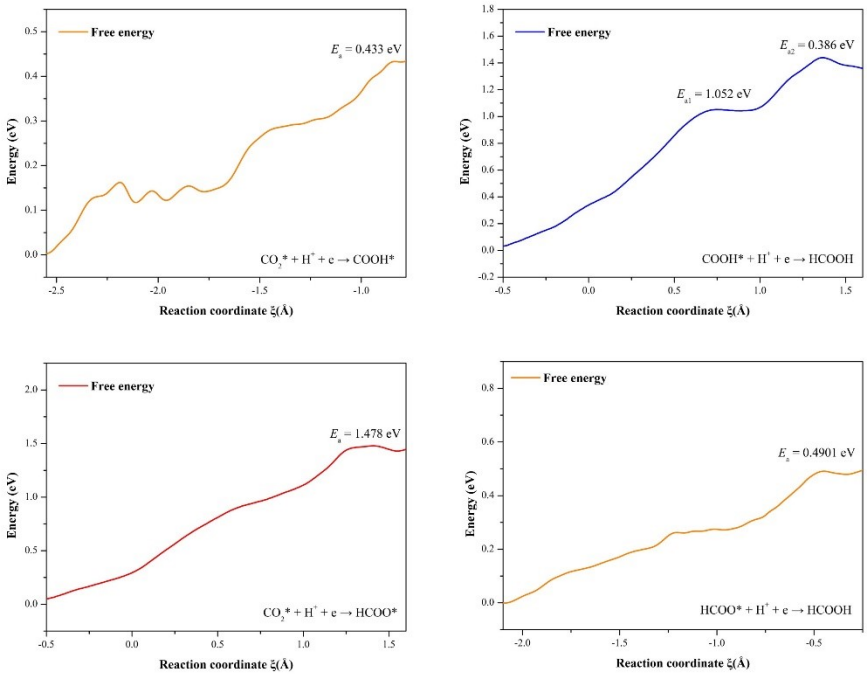

Figure S19 The free energy profiles obtained by integration along the reaction coordinate on Pd_3Au (211).

References

1. D. Y. Jo, H. C. Ham and K.-Y. Lee, *Applied Surface Science*, 2020, **527**, 146857.
2. A. Brown, *Acta Crystallographica*, 1961, **14**, 856-860.
3. J. Kanamori and Y. Kakehashi, *http://dx.doi.org/10.1051/jphyscol:1977754*, 1977, **38**.
4. M. H. F. Sluiter, C. Colinet and A. Pasturel, *Physical Review B*, 2006, **73**, 174204.
5. M. Valenti, N. P. Prasad, R. Kas, D. Bohra, M. Ma, V. Balasubramanian, L. Chu, S. Gimenez, J. Bisquert, B. Dam and W. A. Smith, *ACS Catalysis*, 2019, **9**, 3527-3536.
6. B. Zhu, G. Thrimurthulu, L. Delannoy, C. Louis, C. Mottet, J. Creuze, B. Legrand and H. Guesmi, *Journal of Catalysis*, 2013, **308**, 272-281.
7. F. Gao, Y. Wang and D. W. Goodman, *The Journal of Physical Chemistry C*, 2009, **113**, 14993-15000.
8. D. D. Vasić Anićijević, V. M. Nikolić, M. P. Marčeta Kaninski and I. A. Pašti, *International Journal of Hydrogen Energy*, 2015, **40**, 6085-6096.
9. K. Chan and J. K. Nørskov, *The Journal of Physical Chemistry Letters*, 2015, **6**, 2663-2668.
10. K. Chan and J. K. Nørskov, *The Journal of Physical Chemistry Letters*, 2016, **7**, 1686-1690.
11. R. F. W. Bader, *Chemical Reviews*, 1991, **91**, 893-928.
12. W. Tang, E. Sanville and G. Henkelman, *Journal of Physics: Condensed Matter*, 2009, **21**, 084204.
13. K. Mathew, R. Sundararaman, K. Letchworth-Weaver, T. A. Arias and R. G. Hennig, *Journal of Chemical Physics*, 2014, **140**.
14. K. Mathew, V. S. C. Kolluru, S. Mula, S. N. Steinmann and R. G. Hennig, *Journal of Chemical Physics*, 2019, **151**.
15. T. K. Woo, P. M. Margl, P. E. Blöchl and T. Ziegler, *The Journal of Physical Chemistry B*, 1997, **101**, 7877-7880.
16. H. Oberhofer, C. Dellago and P. L. Geissler, *The Journal of Physical Chemistry B*, 2005, **109**, 6902-6915.
17. C. Jarzynski, *Physical Review Letters*, 1997, **78**, 2690-2693.
18. J. Hafner, *Ab-initio simulations of materials using VASP: Density-functional theory and beyond*, 2008.
19. G. Kresse and J. Furthmüller, *Physical Review B*, 1996, **54**, 11169-11186.
20. G. Kresse and D. Joubert, *Physical Review B*, 1999, **59**, 1758-1775.
21. P. E. Blochl, *Physical Review B*, 1994, **50**, 17953-17979.
22. J. P. Perdew, K. Burke and M. Ernzerhof, *Physical Review Letters*, 1996, **77**, 3865-3868.
23. S. Grimme, S. Ehrlich and L. Goerigk, *Journal of Computational Chemistry*, 2011, **32**, 1456-1465.
24. S. Grimme, J. Antony, S. Ehrlich and H. J. J. o. C. P. Krieg, 2010, **132**, 154104.